New equation of state for astrophysical simulations

G. Shen[*] and C. J. Horowitz[†]

Nuclear Theory Center and Department of Physics, Indiana University, Bloomington, Indiana 47405, USA

S. Teige[‡]

University Information Technology Services, Indiana University, Bloomington, Indiana 47408, USA

We generate a new complete equation of state (EOS) of nuclear matter for a wide range of temperatures, densities, and proton fractions ready for use in astrophysical simulations of supernovae and neutron star mergers. Our previous two papers tabulated the EOS at over 180 000 grid points in the temperature range $T = 0$–80 MeV, the density range $n_B = 10^{-8}$–1.6 fm^{-3}, and the proton fraction range $Y_P = 0$–0.56. In this paper we combine these data points using a suitable interpolation scheme to generate a single EOS table on a finer grid. This table is thermodynamically consistent and conserves entropy during adiabatic compression tests. We present various thermodynamic quantities and the composition of matter in the new EOS, along with several comparisons with existing EOS tables. Our EOS table is available for download.

I. INTRODUCTION

The equation of state (EOS), which is pressure as a function of density and temperature, for warm dense nuclear matter is an important ingredient in the theory of core-collapse supernovae [1]. The EOS influences the shock formation and evolution, and it determines the compactness of the nascent protoneutron star. The EOS also impacts the position of the neutrinosphere, which is the site of last scattering for neutrinos in supernovae, and the emitted neutrino spectra [2]. This helps determine neutrino flavor oscillations [3] and ultimately the spectra of supernova neutrinos in terrestrial detectors.

In a previous paper [4] we used a relativistic mean-field (RMF) model to self-consistently calculate nonuniform matter at intermediate density and uniform matter at high density. In a following paper [5], we used a virial expansion for a nonideal gas of nucleons and nuclei to obtain the EOS at low densities. Our virial approach [6–8] uses elastic scattering phase shifts and nuclear masses as input. We also include Coulomb corrections that can be important for neutrino interactions [9]. Alternative approaches to the EOS at low densities, such as that used in [10], can include model-dependent strong interactions. Altogether our RMF and virial EOS models cover the large range of temperatures, densities, and proton fractions shown in Table I.

Note that pure neutron matter ($Y_P = 0$) is also included in the table. The EOS at zero temperature is obtained by extrapolation from the two lowest temperatures. There are 73 840 data points from the virial calculation at low densities, 17 021 data points from the nonuniform Hartree calculation, and 90 478 data points from uniform matter calculations. The overall calculations took 7000 CPU days using Indiana University's supercomputer clusters.

It is most efficient for astrophysical simulations of supernovae and neutron star mergers to interpolate within an existing EOS table to update the properties of stellar matter with three independent thermodynamics parameters (T, n_B, and Y_P). Therefore in this paper we generate, from these original results, a sufficiently large EOS table that can easily be interpolated in a way that preserves thermodynamic consistency.

There exist only two realistic EOS tables that are in widespread use for astrophysical simulations, the Lattimer-Swesty (L-S) EOS [11], which uses a compressible liquid drop model with a Skyrme force, and the Shen, Toki, Oyamatsu, and Sumiyoshi (S-S) EOS [12,13], which uses the Thomas-Fermi and variational approximations with a RMF model. The two EOSs show clear differences, for example, in the nuclear composition during the core-collapse phase and in the adiabatic index around and above the phase transition to homogeneous nuclear matter [1]. In this paper, we will discuss several comparisons between our new EOS and these two existing ones.

The paper is organized as follows: In Sec. II we present the numerical details for the interpolation scheme we use to generate the full EOS table. Section III shows results for our EOS, including various thermodynamic properties and the composition of matter. The $T = 0$ β equilibrium EOS is also presented and used to calculate the neutron star mass-radius relation. We also give some comparisons between our EOS and the two existing EOS tables. Section IV presents a summary of our results and gives an outlook for future work. In the Appendix the contents of our EOS table are explained in more detail and the public access to our EOS table is given.

This paper presents results based on the relatively stiff RMF interaction of Lalazissis, Konig, and Ring (NL3) [14] that has a high pressure at high densities. In later work we will present additional EOS tables for other softer interactions. This will allow one to more easily run astrophysical simulations for different EOS tables and identify quantities that are sensitive to the EOS. Note that a variety of uncertainties in the EOS and

_____

[*]gshen@indiana.edu
[†]horowit@indiana.edu
[‡]steige@indiana.edu

TABLE I. Range of temperature T, baryon density n_B, and proton fraction Y_P in the EOS table.

Parameter	Minimum	Maximum	Number of points
T (MeV)	$0, 10^{-0.8}$	$10^{1.9}$	36
$\log_{10} n_B$ (fm^{-3})	-8.0	0.2	83
Y_P	$0, 0.05$	0.56	53

TABLE II. Range of temperature T, baryon density n_B, and proton fraction Y_P in the finely spaced interpolated EOS table.

Parameter	Minimum	Maximum	Number of points
T (MeV)	$0, 10^{-0.8}$	$10^{1.9}$	110
$\log_{10} n_B$ (fm^{-3})	-8.0	0.2	329
Y_P	$0, 0.05$	0.56	$1(Y_P = 0) + 52$

some laboratory measurements and astronomical observations related to the EOS have been discussed in our previous papers [4,5].

II. NUMERICAL DETAILS

In this section we describe how we interpolate our free energy results and calculate other quantities from derivatives of the free energy in a thermodynamically consistent manner.

A. Equation of state at zero temperature

At sub-MeV temperatures, the EOS is not very sensitive to variation in the temperature. In our calculations, the ($T = 0$)

EOS is obtained by quadratic extrapolation from the results at the two lowest temperatures $T = 0.158$ and 0.251 MeV [15]. Specifically, thermodynamic quantities (such as the free energy) have the approximate temperature dependence

$$F(T) = F(T = 0) + aT^2, \qquad (1)$$

and this equation is used to find $F(T = 0)$.

We start with the $T = 0$ part of the EOS that constitutes the most important contribution to the adiabatic index Γ and the speed of sound, particularly at low temperature. The latter two quantities mostly rely on the derivative $(dP/dn)|_T$, which involves a second derivative of free energy with respect to density and this is sensitive to noise in the bicubic interpolation scheme that we use. We start from the original Table I, which
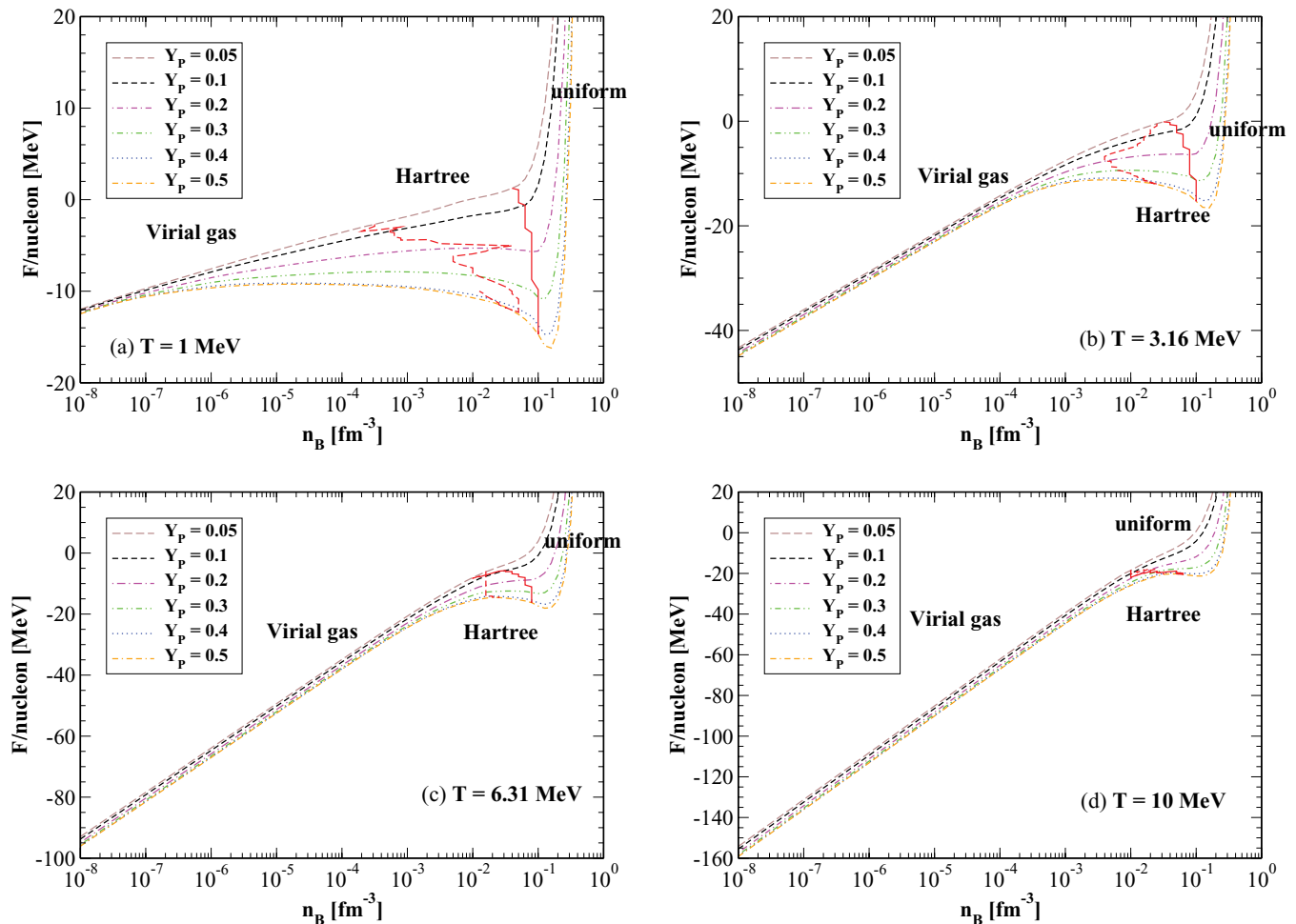

FIG. 1. (Color online) Free energy per nucleon of nuclear matter at temperatures T of (a) 1, (b) 3.16, (c) 6.31, and (d) 10 MeV. The proton fraction ranges from $Yp = 0.05$ to 0.5.

is used to generate the pressure at $T = 0$ (and we also include the electron pressure in the following smoothing procedure). The thermodynamic pressure P_{th} can be obtained numerically from the free energy per baryon, F/A,

$$P_{th} = n_b^2 \left(\frac{\partial(F/A)}{\partial n_b} \right)_{T, Y_p}. \tag{2}$$

We smooth the pressure in a 10 points per decade table by removing points that differ significantly from the geometric mean of neighboring points and replace them with interpolated values. Then we use monotonic cubic Hermite interpolation [16] on the smoothed table of pressure to get a finer table with 40 points per decade in the density axis. Finally, we obtain the (free) energy at zero temperature by integrating this pressure with respect to density.

B. The entropy at finite temperature

Next, we calculate the entropy at finite temperatures $T < 12.5$ MeV. From the free energy points at temperature T, density n_B, and proton fraction Y_P as in Table I, the entropy per baryon, s_{th}, can be obtained numerically as

$$s_{th} \equiv S/A = -\left(\frac{\partial(F/A)}{\partial T} \right)_{n_b, Y_p}. \tag{3}$$

Finally, the energy per baryon, e_{th}, is

$$e_{th} = F/A - T s_{th}. \tag{4}$$

Note that for higher temperatures $T \geqslant 12.5$ MeV, matter is uniform for all proton fractions and densities. For uniform matter, all thermodynamic quantities can be obtained directly from RMF calculations, with good thermodynamic consistency.

The bicubic interpolation scheme we use does not guarantee the monotonicity of the second derivative, e.g.,

$$\frac{\partial S}{\partial T} = -\frac{\partial^2 F}{\partial^2 T} \geqslant 0. \tag{5}$$

As a result, the internal energy per baryon, e_{th}, is not guaranteed to be monotonic either:

$$\frac{\partial e_{th}}{\partial T} \geqslant 0. \tag{6}$$

The bicubic interpolation with slope limiter can guarantee that the free energy is monotonic and that the first law of thermodynamics will be satisfied. But it is not sufficient to preserve monotonicities of the entropy and internal energy, nor can it guarantee smoothness of $(dP/dn)|_T$.

The following scheme is used to generate a big table of EOSs that are thermodynamically consistent, keeping monotonicities of entropy and energy, and preserving the smoothness of $(dP/dn)|_T$. We start with the entropy in the (T, n_b) plane as in Table I with 10 points per decade of density and temperature. Then we sweep through the raw table of entropy, discarding numerically noisy points that violate the following constraints:

$$\frac{\partial S}{\partial T} > 0, \qquad \frac{\partial S}{\partial n} < 0. \tag{7}$$
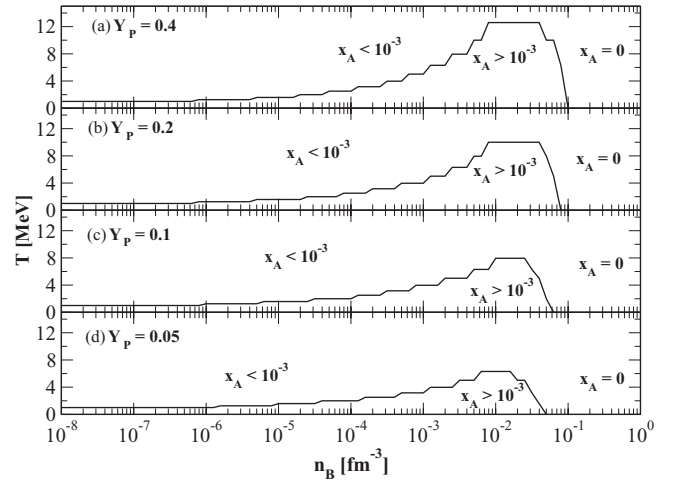

FIG. 2. Phase diagram of nuclear matter at proton fractions Y_P of (a) 0.4, (b) 0.2, (c) 0.1, and (d) 0.05. X_A is the mass fraction of heavy nuclei with mass number $A > 4$.

We replace those points by interpolation from neighboring points. Therefore we have a table of entropy that satisfies conditions in Eq. (7). (The electron and photon parts can be handled more accurately, by monotonic interpolation on individual quantities such as energy, pressure, and entropy.) Then we further smooth the entropy as a function of density while keeping Eq. (7) by further replacing noisy points with interpolated values. This procedure ensures the smoothness of $(dP/dn)|_T$.

Now we perform monotonic cubic Hermite interpolation on this small table of entropy with 10 points per decade to generate a larger EOS table with 40 points per decade in both the temperature and density directions, as indicated in Table II. Then we integrate this smoothed entropy table as a function of temperature to get values of the free energy (adding the energy at zero temperature to make the full free energy). Thus we obtain the free energy on this finer 40 by 40 points per decade grid in a thermodynamically consistent fashion.
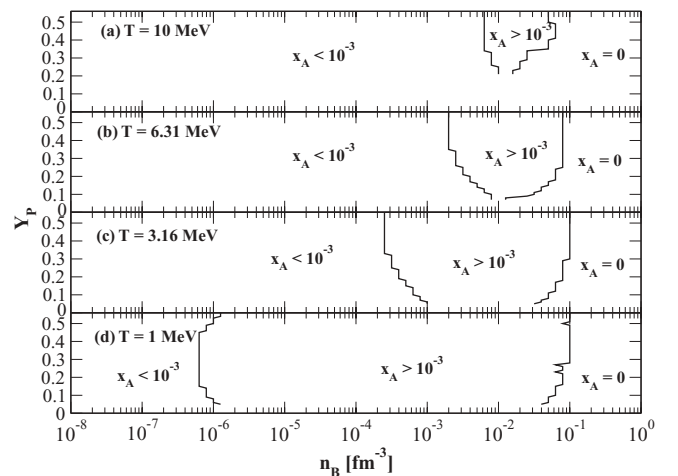

FIG. 3. Phase diagram of nuclear matter at temperatures of (a) 10, (b) 6.31, (c) 3.16, and (d) 1 MeV. X_A is the same as in Fig. 2.
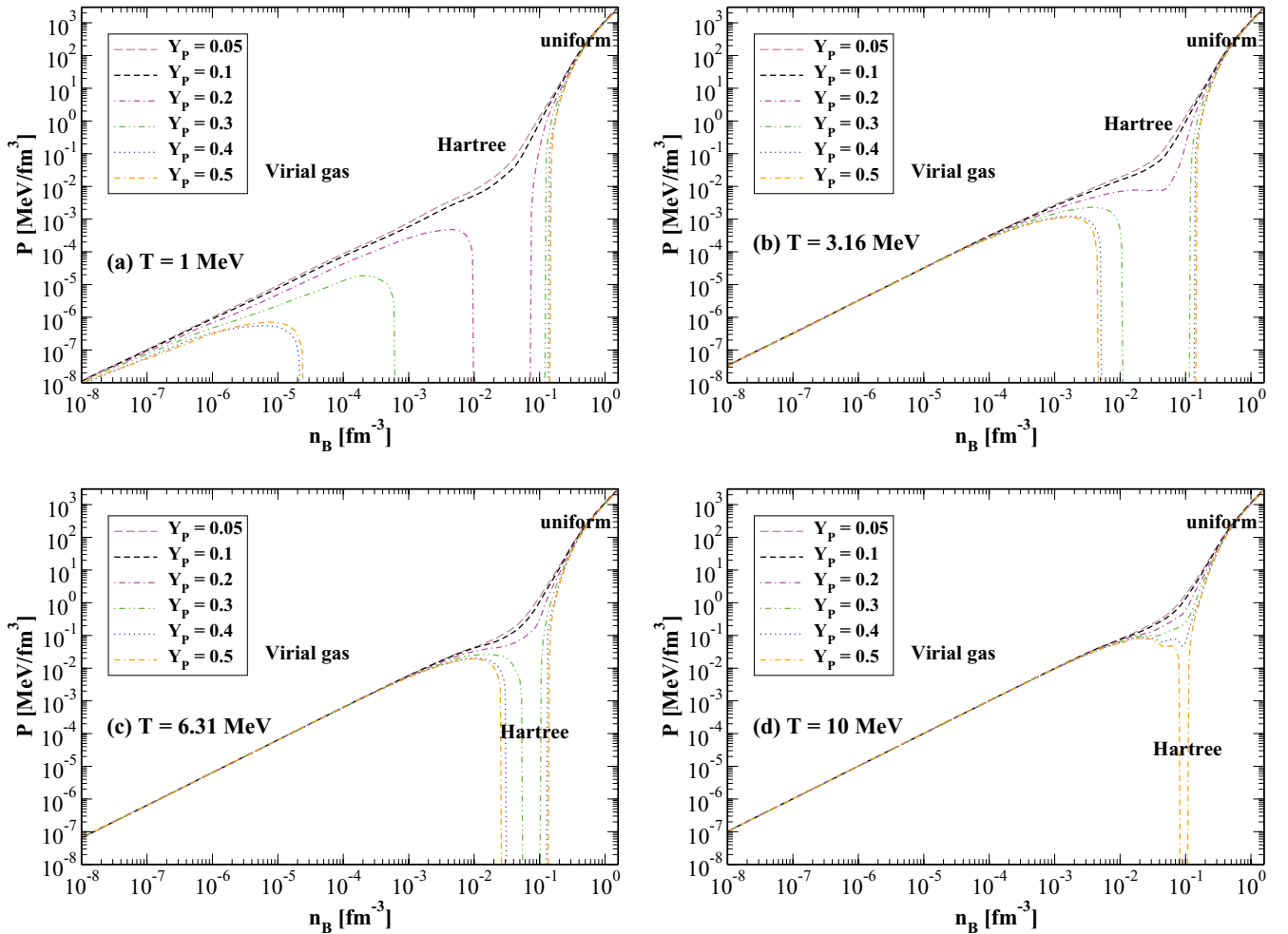
FIG. 4. (Color online) Pressure of nuclear matter at temperatures of (a) 1, (b) 3.16, (c) 6.31, and (d) 10 MeV. The proton fraction ranges from $Y_P = 0.05$ to 0.5.

C. Bicubic Interpolation of F/A

The final step is to carry out bicubic interpolation of the previous free energy values (as in Table II) to generate the entropy and pressure by the thermodynamic derivatives in Eqs. (2) and (3). This prescription guarantees the monotonicity of entropy and pressure in the final table and conserves the first law of thermodynamics in adiabatic compression tests.

We first apply bicubic interpolation [17] for the free energy. The first derivatives on the grid points are generated from monotonic cubic Hermite interpolation [16]. The second derivative (the cross derivative) $\partial^2 F/\partial n \partial T$ on the grid points is generated as in Ref. [17]. The bicubic interpolation can then fit free energies with cubic functions in temperature and density coordinates and provides the first and second (cross) derivatives. Then the entropy and pressure are obtained from Eqs. (2) and (3). Finally, the boundary points at the highest temperature or density are discarded to avoid boundary artifacts in the interpolation.

III. RESULTS FOR THE EQUATION OF STATE

In this section we discuss various thermodynamic quantities and the composition of matter in the EOS. First, we discuss the free energy per baryon from virial gas, nonuniform Hartree mean-field, and uniform matter calculations. Next we map out the phase boundaries of our EOS. Then we show various thermodynamic quantities, such as the pressure, entropy per baryon, chemical potentials of neutrons, protons, and electron neutrinos, and adiabatic index. We also show information on the composition, i.e., the average mass number and proton number of heavy nuclei in nonuniform matter, and the mass fractions of different species. The zero-temperature EOS in chemical equilibrium is presented next, and this is used to calculate neutron star structure. Finally, we make some comparisons between our EOS and those of L-S [11] and S-S [13].

A. Free energy and phase boundaries

In Fig. 1, the free energy per baryon, F/A, for matter at $T = 1$, 3.16, 6.31, and 10 MeV with different proton fractions is shown as a function of density n_B. The free energy F/A is obtained from virial gas, nonuniform Hartree mean-field, and uniform matter calculations, respectively. In most cases the transition (as the density grows) is found at the density where Hartree calculations or uniform matter calculations give the lowest free energy. For matter at very low temperature (not
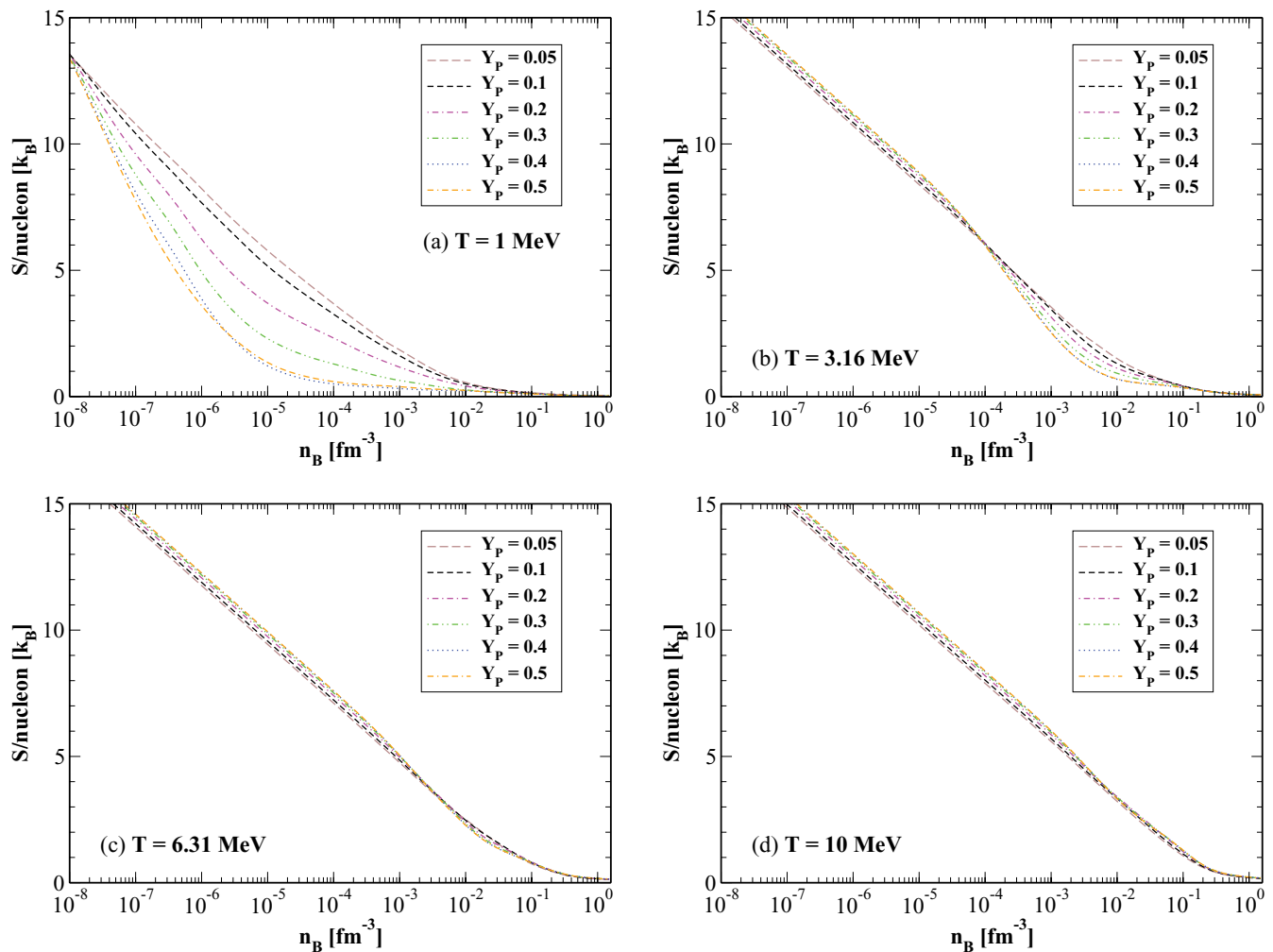
FIG. 5. (Color online) Entropy per nucleon of nuclear matter at temperatures of (a) 1, (b) 3.16, (c) 6.31, and (d) 10 MeV. The proton fraction ranges from $Y_P = 0.05$ to 0.5.

greater than ∼1 MeV) and low proton fraction (not greater than ∼0.1), some matching points are obtained at densities where virial gas and Hartree calculations give the closest free energies. (The difference is less than hundreds of keV, and note that the mass table [18] used in our virial EOS [5] has itself 600-keV rms deviations in nuclear binding energies compared to data.) Detailed information has been reported in our previous paper [5]. We reproduce the figure here for completeness.

In Fig. 2, we show the phase boundaries of nuclear matter at different proton fractions $Y_P = 0.05, 0.1, 0.2$ and 0.4. The mass fraction of heavy nuclei with mass number $A > 4$ is X_A. The boundary at low densities indicates when X_A is greater or less than 10^{-3}. The boundary at high densities indicates the transition between nonuniform matter and uniform matter. At very low densities, the matter is dominated by free nucleons and α particles. As the density rises, heavy nuclei persist to higher temperatures. Finally, uniform matter takes over at sufficiently high density. Figure 2 also shows that, as proton fraction rises, the temperature regime with appreciable heavy nuclei grows and the transition density to uniform matter increases. The density for the nonuniform matter to

uniform matter transition has a weak temperature dependence. Figure 3 shows the phase diagram of nuclear matter at different temperatures $T = 1, 3.16, 6.31$, and 10 MeV. Similarly, as in Fig. 2, the left boundary at low density indicates where X_A is greater or less than 10^{-3}. The right boundary at high density indicates the transition between nonuniform matter and uniform matter. As the temperature grows, the Y_P dependence of the phase boundaries becomes larger, and the density regime with appreciable heavy nuclei rapidly shrinks. Our Figs. 2 and 3 are very similar to the corresponding Figs. 2 and 3 of [13] for the S-S EOS.

B. Pressure

In Fig. 4, the pressure of nuclear matter with different proton fractions is shown as a function of density, for four different temperatures (1, 3.16, 6.31, and 10 MeV). The pressure is obtained via the bicubic Hermite interpolation in Eq. (2). For matter at low density in the virial gas phase, the pressure scales nicely with density. When the density increases, formation of additional nuclei decreases the pressure. The Coulomb
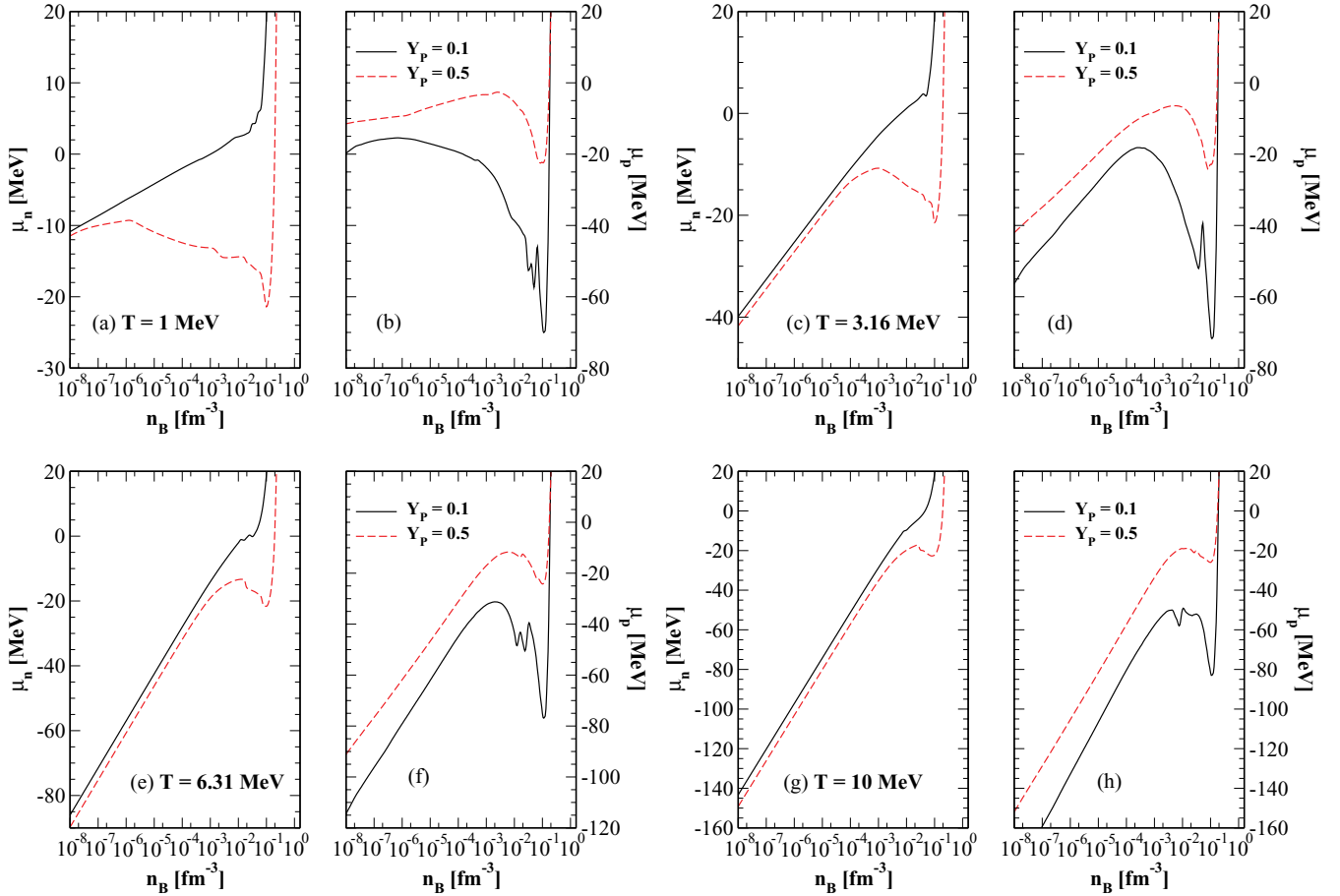
FIG. 6. (Color online) Chemical potentials of neutrons and protons at different temperature and proton fractions.

correction to the lattice energy reduces the pressure even further. Note in part of the virial gas and Hartree Wigner-Seitz cell regions, the pressure is negative. Figure 4 only shows the hadronic contribution to the pressure. In addition one needs to take into account the contribution from electrons and photons, which makes the total pressure (not shown here) positive. We also note that with inclusion of electrons and photons in the final table, the condition for thermodynamic stability against density fluctuations is always preserved to the numerical precision of the table,

$$\frac{dP}{dn}\bigg|_T \geqslant 0. \tag{8}$$

Finally, after the Hartree to uniform matter transition, the pressure rises rapidly with density because of the large incompressibility of nuclear mater.

C. Entropy

In Fig. 5(a), the entropy per baryon is shown as a function of density for nuclear matter with $T = 1$ MeV at different proton fractions. The entropy is calculated from Eq. (3). Near a density of a few times 10^{-8} fm^{-3}, the entropy drops rapidly with density, which indicates formation of nuclei, first mostly α particles and then heavier nuclei at higher density.

Later we will illustrate this by plotting the mass fractions of different species. For nuclear matter with a large proton fraction, larger mass fractions of heavy nuclei are present so that the entropy drops more rapidly with density. When nuclei comprise more than 90% of the mass fraction, the entropy remains almost constant as the density increases. Figures 5(b), 5(c), and 5(d) show the entropy per baryon in nuclear matter at higher temperatures of 3.16, 6.31, and 10 MeV. They have characteristics similar to those for $T = 1$ MeV, except that the range of densities where the entropy drops rapidly, due to formation of nuclei, becomes smaller because it is harder to form heavy nuclei at higher temperatures.

D. Chemical potentials of *n*, *p*, and *ν_e*

In Fig. 6, the neutron [left sketches (a), (c), (e), and (g)] and proton [right sketches (b), (d), (f), and (h)] chemical potentials are shown for nuclear matter with $Y_p = 0.1$ (black curves) and 0.5 (red curves) at different temperatures. For nuclear matter at low density and/or high temperature, the chemical potentials scale with density. The formation of nuclei breaks the scaling behavior; i.e., the bound nucleons have much smaller chemical potentials.

In Fig. 7, the equilibrium electron-neutrino chemical potential, defined as $\mu_{\nu_e} \equiv \mu_e + \mu_p - \mu_n$, is shown versus
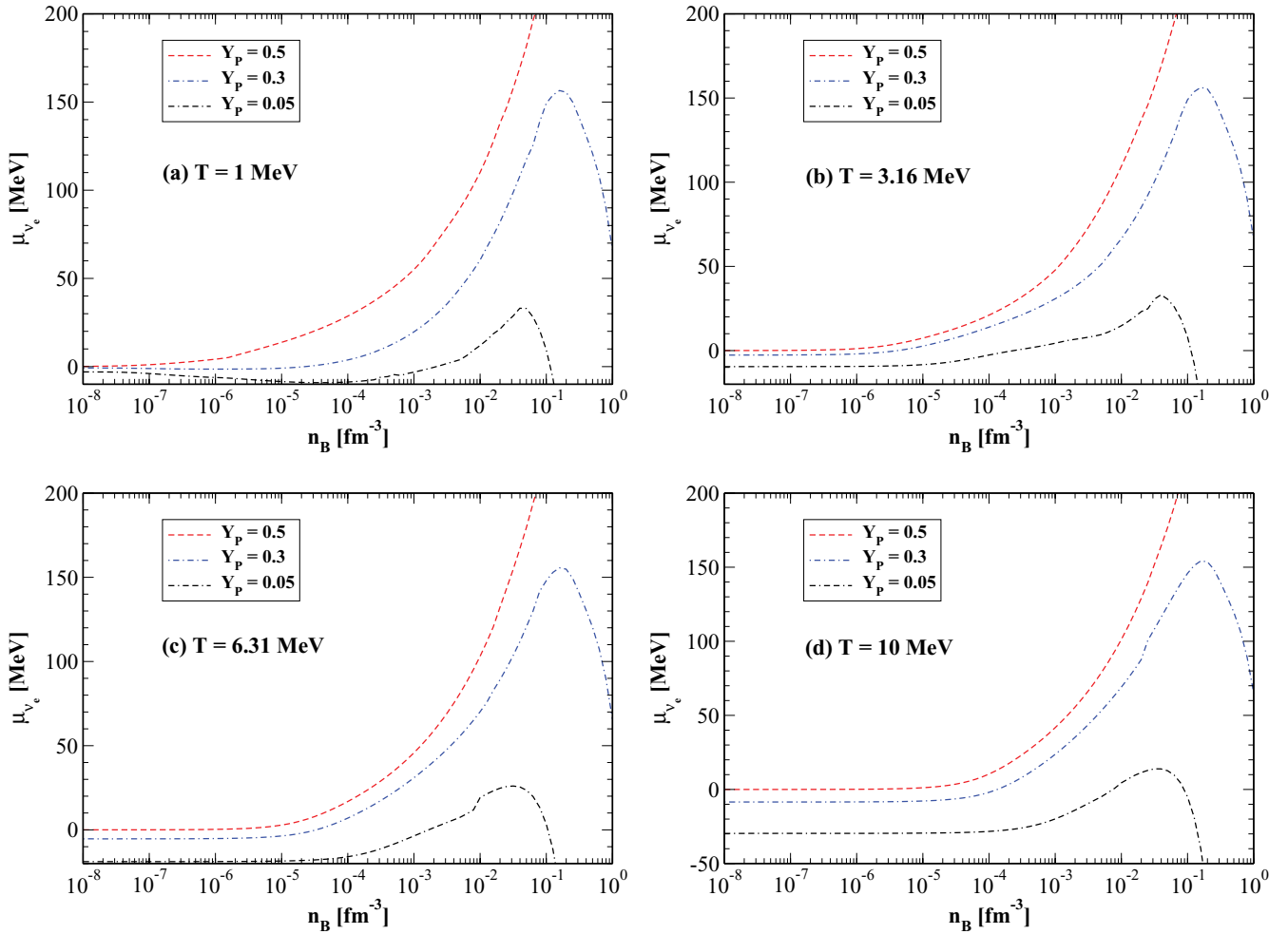
FIG. 7. (Color online) Equilibrium electron-neutrino chemical potential μ_{ν_e} for nuclear matter at various temperatures and proton fractions. The potential is defined as $\mu_{\nu_e} \equiv \mu_e + \mu_p - \mu_n$.

density for nuclear matter at various temperatures and proton fractions. Let us focus on Fig. 7(a) where nuclear matter has $T = 1$ MeV. For symmetric nuclear matter, μ_{ν_e} grows rapidly with density, since μ_p almost cancels μ_n and $\mu_{\nu_e} \sim \mu_e \sim n_B^{1/3}$. For proton-rich nuclear matter ($Y_P > 0.5$), μ_{ν_e} will grow even faster than for symmetric nuclear matter. For neutron-rich nuclear matter, μ_{ν_e} has a maximum value at some density. This is due to the competition between the electron chemical potential and the difference between the proton and neutron chemical potentials. The latter difference between proton and neutron is negative when the proton fraction is less than 0.5. The density where μ_{ν_e} has a maximum decreases with decreasing proton fraction. It is ~ 0.2 fm^{-3} when $Y_P = 0.3$, and ~ 0.05 fm^{-3} when $Y_P = 0.05$. In the limit of pure neutron matter there is no maximum for μ_{ν_e}, which is just negative μ_n by construction.

E. Adiabatic index Γ_s

The left panel of Fig. 8 shows the temperature of the adiabat with constant entropy $S = 1$ for nuclear matter with proton

fraction $Y_P = 0.1, 0.2, 0.3$, and 0.4 including baryon, electron, positron, and photon contributions to S. At low density, matter is dominated by free nucleons in the gas phase. There are lots of kinetic degrees of freedom and one needs only a small temperature for the matter to have $S = 1$. When the density rises, the formation of heavy nuclei suppresses the entropy, and it takes higher temperatures for the matter to reach $S = 1$. The entropy, in this case, comes from a fraction of free nucleons in a gas and the partial occupation of levels in the heavy nuclei. When uniform nuclear matter forms at high density, it takes even a higher temperature to reach the same entropy $S = 1$ because the uniform matter is highly degenerate and the entropy comes only from excitations above the Fermi surfaces.

The adiabatic index

$$\Gamma_s = \left(\frac{\partial \ln P}{\partial \ln n} \right)_s \qquad (9)$$

describes the stiffness of the EOS at constant entropy. In the right panel of Fig. 8, the adiabatic index is shown versus density for nuclear matter again including baryon, electron, positron, and photon contributions with constant entropy $S = 1$ and
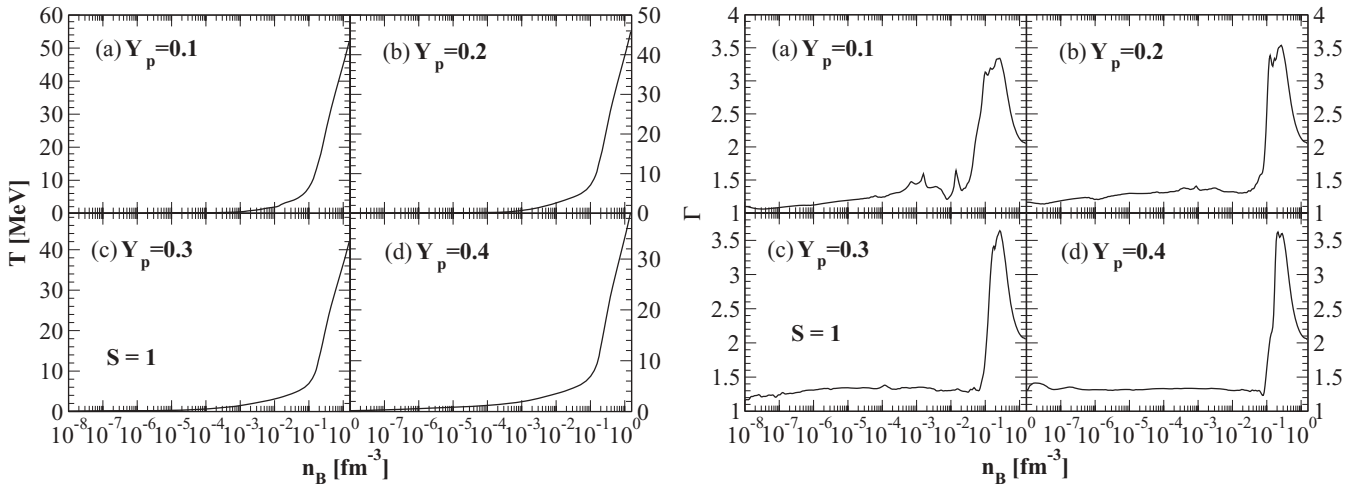
FIG. 8. (Color online) Left: Temperature along the adiabat with constant entropy $S = 1$ for nuclear matter, including baryon, electron, positron, and photon, and proton fractions Y_P of (a) 0.1, (b) 0.2, (c) 0.3, and (d) 0.4. Right: Adiabatic index for nuclear matter, including baryon, electron, positron, and photon, with constant entropy $S = 1$ and proton fractions of (a) 0.1, (b) 0.2, (c) 0.3, and (d) 0.4.

$Y_P = 0.1$, 0.2, 0.3, and 0.4. At subnuclear density, Γ_s remains almost constant with small variations. It then rises rapidly at the transition from nonuniform to uniform matter. This characterizes the stiffening of the EOS due to the large nuclear incompressibility at high density.

F. Average $\bar{A}$ and $\bar{Z}$ of heavy nuclei

Figure 9 shows the average mass number $\bar{A}$ of heavy nuclei (with $A > 4$) versus baryon density at different temperatures and proton fractions. Note that α particles are not counted as heavy nuclei. Let us first look at Fig. 9(a), where $T = 1$ MeV. Nuclear shell effects give rise to several approximate plateaus in $\bar{A}$ versus density for each Y_P, for example, $\bar{A} = 12$, $\sim$50, $\sim$80, and $\sim$100. Usually $\bar{A}$ is larger in matter with smaller Y_P. There are oscillations in $\bar{A}$ in the Hartree mean-field regime. This is due to both nuclear shell effects and small errors in the free energy minimization due to our using a finite step in the Wigner-Seitz cell size [4]. The average mass $\bar{A}$ can be as large as 3000 at high density before the final transition to uniform matter. At higher temperatures, as shown in the other sketches of Fig. 9, $\bar{A}$ grows more rapidly to several thousand in narrower ranges of density. As a result, the width of the plateaus in $\bar{A}$ with density become much shorter and finally vanish.

Figure 10 shows the average proton number $\bar{Z}$ of heavy nuclei versus baryon density at different temperatures and proton fractions. The average proton number has very similar characteristics to those for the average mass number, except that the differences in $\bar{Z}$ between different Y_P are smaller.

G. Mass fractions of nucleons and different nuclei

In Fig. 11, the mass fractions of free neutrons, free protons, α particles, and heavy nuclei are shown versus baryon density

at four different temperatures for a proton fraction $Y_P = 0.05$. The matter is extremely neutron rich, so the mass fraction of free neutrons is always appreciable at any density. Note that in the Hartree mean-field results, there is only a single nucleus associated with each Wigner-Seitz cell. We define a nucleon level to be free when it has positive energy. In Fig. 11(a), $T = 1$ MeV. At very low densities (less than a few times 10^{-8} fm^{-3}), the system is basically a free neutron and proton gas. The α fraction rises rapidly to 10% around a density of 10^{-7} fm^{-3}. Some of the free neutrons are used to form α particles, so the fraction of free neutrons drops to 90%. The free neutron fraction drops further beyond a density of 10^{-6} fm^{-3}, where heavy nuclei appear with a mass fraction of about 15%. The fraction of heavy nuclei grows faster after the virial-gas–Hartree-mean-field transition around 3×10^{-4} fm^{-3}. More and more free neutrons are bound to form heavier nuclei, as can be seen in Fig. 9. The fraction of heavy nuclei reaches a maximum value of 70% before the final transition to uniform matter. Figures 11(b), 11(c), and 11(d) give the mass fractions of the different species at higher temperatures. In these cases, the appearance of α particles and heavy nuclei occurs at higher densities and with smaller mass fractions compared to the $T = 1$ MeV case. When $T = 6.31$ MeV, there is only a narrow range of densities where α particles have a mass fraction of a couple of percent and the amount of heavy nuclei is very small.

Figures 12 and 13 show the mass fractions that were shown in Fig. 11, but for matter with higher proton fractions $Y_P = 0.2$ and 0.5, respectively. The α particles appear at densities similar to those for $Y_P = 0.05$, but with much larger mass fractions. For example, the α fraction can almost reach 100% around 10^{-6} fm^{-3} when $T = 1$ MeV and $Y_P = 0.5$. Heavy nuclei also appear at densities for $Y_p = 0.05$, and with much larger mass fractions. As the proton fraction rises, heavy nuclei can survive to higher temperatures, even though only at very high density. For example, when $T = 10$ MeV and $Y_P = 0.5$, heavy
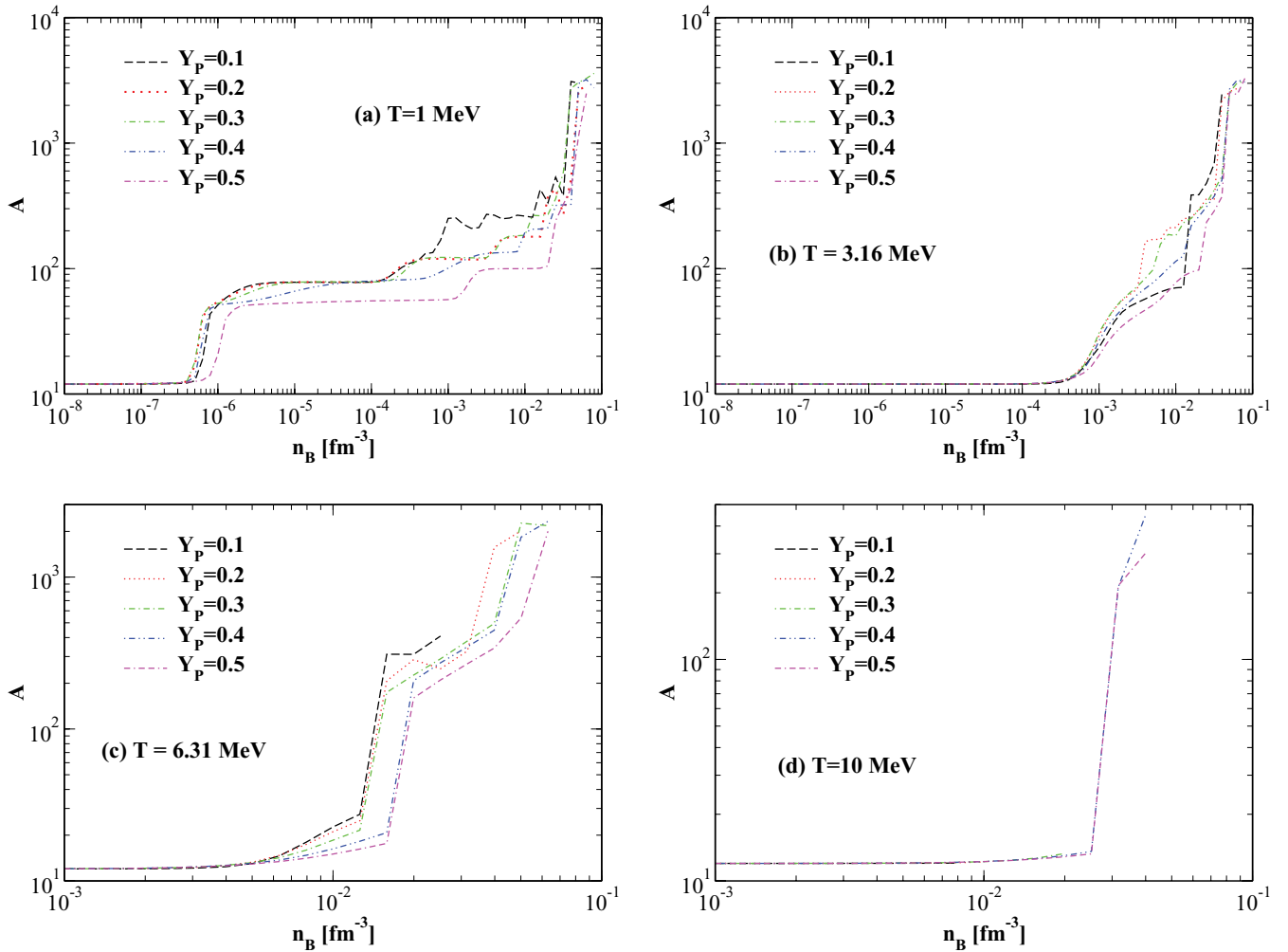
FIG. 9. (Color online) Average mass number of heavy nuclei at temperatures of (a) 1, (b) 3.16, (c) 6.31, and (d) 10 MeV. The proton fraction ranges from $Y_P = 0.1$ to 0.5.

nuclei have a large mass fraction for densities of around a few times 10^{-2} fm^{-3}.

H. β equilibrium at zero temperature

Matter in β equilibrium at zero temperature is particularly interesting and determines neutron star structure, including the mass-radius relation and the neutron star crust. The $T = 0$ EOS is included in our Table II, which can be used to find the β equilibrium EOS by imposing the constraint $\mu_n = \mu_p + \mu_e$. The resulting energy per baryon, pressure, and proton fraction are shown as functions of density in Fig. 14. The energy per baryon starts near -8.5 MeV, which is a typical value for stable nuclei, at 10^{-8} fm^{-3}, becomes positive around 10^{-3} fm^{-3}, and finally rises rapidly after the transition to bulk uniform matter at around 0.05 fm^{-3}. The pressure versus density is polytropic-like below 10^{-4} fm^{-3}, and then it develops small plateaus. After the transition to uniform matter, the pressure rises more rapidly, which indicates a stiffening of the EOS. At 10^{-8} fm^{-3} matter is made up of stable nuclei with similar numbers of neutrons and protons. That is why the proton fraction at 10^{-8} fm^{-3} is as high as 0.45. The proton fraction

drops as the density increases, which means matter becomes more and more neutron rich due to the large electron Fermi energy. The proton fraction reaches a minimum value of 0.007 around 0.025 fm^{-3}. However, it increases again due to the large symmetry energy at high density for the NL3 [14] interaction, which favors more nearly equal neutron and proton fractions.

I. Neutron star structure

The mass and radius of a neutron star are obtained by solving the Tolman-Oppenheimer-Volkoff (TOV) equations [19,20].

By using the EOS in β equilibrium at zero temperature from the previous Sec. III H in the core and using the Baym-Pethick-Sutherland EOS in the crust [21], we obtain the neutron star mass-radius and mass-central density relations, which are plotted in Fig. 15. The neutron star's maximum gravitational mass is about 2.77 solar mass with a radius of 13.3 km. The corresponding central density is about 10^{15} g/cm^3. The large value for the maximum neutron star mass is not too surprising since NL3 provides a very stiff EOS as we have emphasized several times.
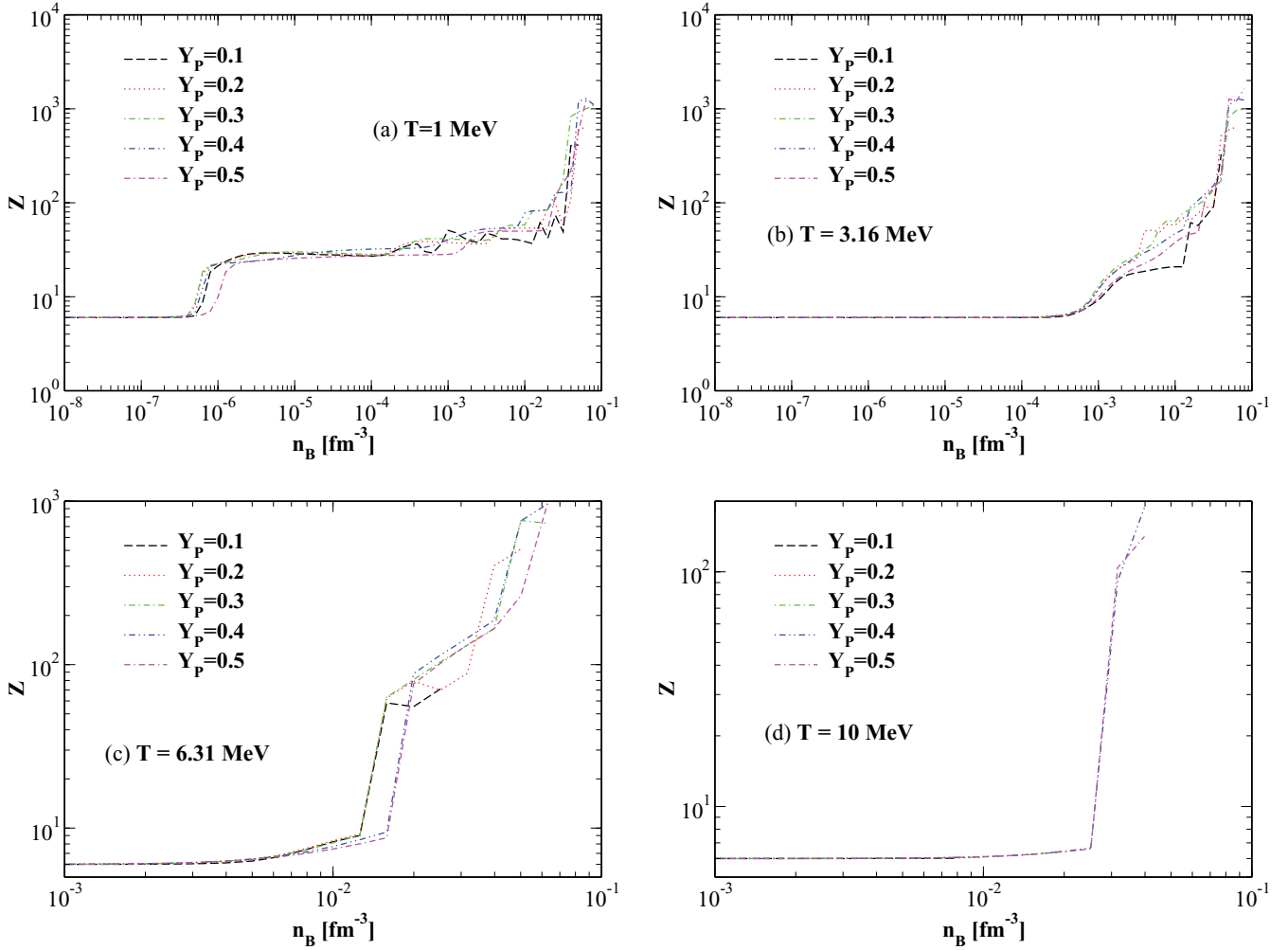
FIG. 10. (Color online) Average proton number of heavy nuclei at temperatures of (a) 1, (b) 3.16, (c) 6.31, and (d) 10 MeV. The proton fraction ranges from $Y_P = 0.1$ to 0.5.

J. Comparisons with the L-S and S-S EOSs

It is instructive to compare our EOS with the L-S EOS, which uses a simple liquid drop model with a nonrelativistic Skyrme interaction, and the S-S EOS, which uses the Thomas-Fermi and variational approximations to a RMF model. The L-S EOS quoted in this work corresponds to the one with incompressibility coefficient $K = 180$ MeV. In Fig. 16, the pressure for matter at $T = 1$ or 6.31 MeV and $Y_P = 0.05$ or 0.4 is shown for our, L-S's, and S-S's EOSs. Here the pressure includes contributions from electrons, positrons, and photons. Below nuclear saturation density ($\sim$0.16 fm^{-3}), ours and S-S's EOSs agree very well. The L-S EOS gives a slightly lower pressure at densities above 10^{-3} fm^{-3} when $T = 1$ MeV and $Y_P = 0.05$. Above saturation density, our EOS gives the largest pressure.

Figure 17 compares the mass fraction of heavy nuclei from our, L-S's, and S-S's EOSs for matter at $T = 1$ or 6.31 MeV and $Y_P = 0.05$ or 0.4. Although the pressure agrees well among the three EOSs, the mass fraction of heavy nuclei and α particles can be different and this contributes to the differences in entropy shown in Fig. 18. In addition, our EOS

may have a higher entropy in Fig. 18(b), because we may have smaller nuclei for n less than 10^{-3} fm^{-3} compared to the S-S EOS, and because we can have a distribution of several heavy nuclei, while the L-S and S-S EOSs use only a single average species. The average A and Z of heavy nuclei are shown in Fig. 19. This figure clearly shows the effects of shell structure that are included in our EOS but are neglected in both L-S and S-S EOSs. As a result, A and Z for our EOS have a series of steps while A and Z for the L-S and S-S EOSs increase smoothly with density.

For $T = 1$ MeV and $Y_P = 0.05$, the three EOSs agree very well on entropy, except that at low densities the L-S EOS gives a slightly smaller value. It is comprehensible since the matter is dominated by free neutrons until very high density when heavy nuclei dominate [Fig. 17(a)]. But heavy nuclei have low entropy at low temperatures so the difference in entropy between the EOSs is small. For $T = 1$ MeV and $Y_P = 0.4$, the differences in entropy among the three EOSs are larger. This is partially due to the smaller scale used. It is also because the different EOSs predict different mass fractions of heavy nuclei, whose formation decreases the entropy. The L-S EOS
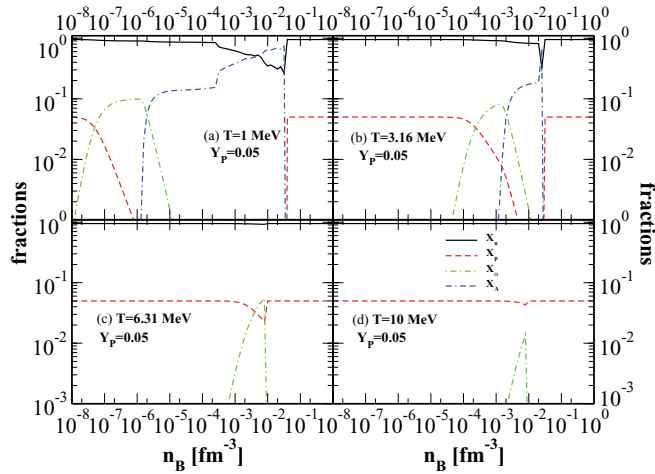
FIG. 11. (Color online) Mass fractions of free neutrons, free protons, α particles, and heavy nuclei vs baryon density at temperatures of (a) 1, (b) 3.16, (c) 6.31, and (d) 10 MeV and fixed proton fraction $Y_P = 0.05$.

FIG. 13. (Color online) Mass fractions of free neutrons, free protons, α particles, and heavy nuclei vs baryon density at temperatures of (a) 1, (b) 3.16, (c) 6.31, and (d) 10 MeV and fixed proton fraction $Y_P = 0.5$.

has 80% heavy nuclei at 10^{-6} fm^{-3} [Fig. 17(b)] compared to 20% in our EOS and the S-S EOS; therefore, the L-S EOS has the lowest entropy. At the higher temperature $T = 6.31$ MeV, the three EOSs agree well on entropy for different values of Y_P, because free nucleons dominate at most densities [Figs. 17(c) and 17(d)].

The differences in abundances and average A and Z between EOSs may arise because of differences in symmetry energy and approximations made. For example, the L-S EOS uses a very simple liquid drop model while the S-S EOS uses variational and Thomas-Fermi approximations that are avoided in our EOS. These differences could be important for neutrino interactions and should be studied further.
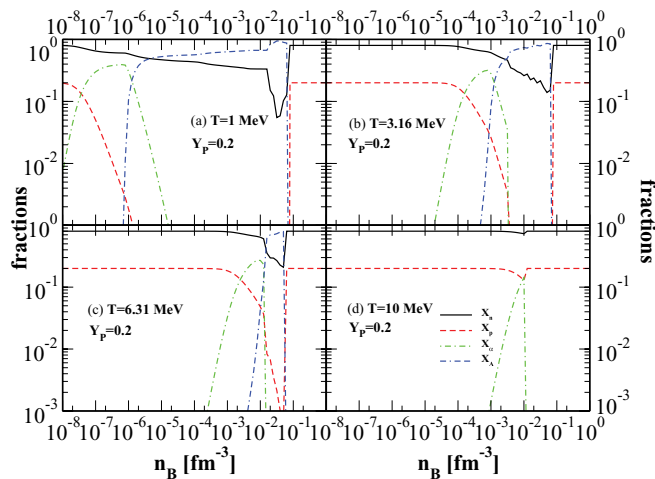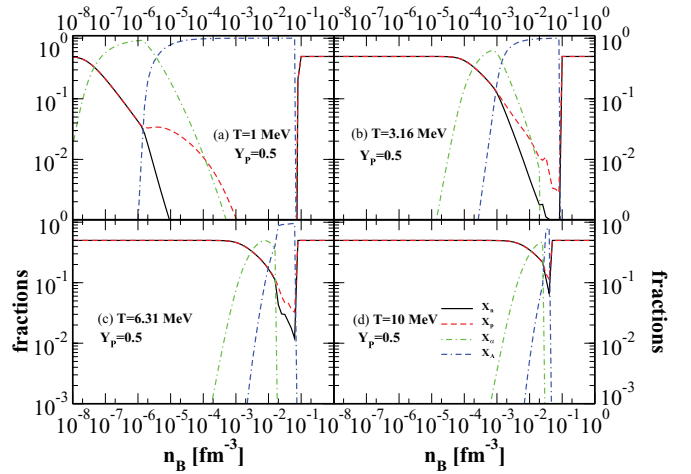

FIG. 12. (Color online) Mass fractions of free neutrons, free protons, α particles, and heavy nuclei vs baryon density at temperatures of (a) 1, (b) 3.16, (c) 6.31, and (d) 10 MeV and fixed proton fraction $Y_P = 0.2$.

K. Adabatic compression tests

One important test of thermodynamic consistency for our EOS table is to check that entropy is conserved as matter undergoes adiabatic compression. This is very closely related to the conservation of energy in the first law of thermodynamics. Let us consider the following adiabatic compression procedure.

 (i) Start from an energy per baryon, $E[n(t_0), T(t_0)]$, a density $n(t_0)$, and a temperature $T(t_0)$. Here t stands for a sequence of times starting at t_0. The pressure P is then given by the EOS.

 (ii) Now compress the matter by increasing the density by an amount dn so that $n(t_1) = n(t_0) + dn$ with $t_1 = t_0 + 1$.

(iii) Next ensure that the first law of thermodynamics is satisfied by using a backward-difference equation and requiring

$$E[n(t_1), T(t_1)] = E[n(t_0), T(t_0)] + P[n(t_1), T(t_1)]\, dn \tag{10}$$

by solving for the new pressure $P[n(t_1), T(t_1)]$ and temperature $T(t_1)$.

(iv) Finally, the updated entropy $S[n(t_1), T(t_1)]$ follows from our EOS at the new density $n(t_1)$ and temperature $T(t_1)$.

The entropy should be conserved in this adiabatic compression so that S is independent of t. In Fig. 20, the temperature and entropy versus density during adiabatic compression are shown for nuclear matter with fixed proton fraction $Y_P = 0.15$. The initial density is $5.167\,38 \times 10^{-6}$ fm^{-3} and initial temperature is 0.5 MeV. The solid curve is a test result for our EOS table with lepton and photon contributions included in addition to contributions from baryons. The dashed curve is a test result for our EOS table with baryons alone. The variation in entropy for both cases is less than 1%. For a comparison the
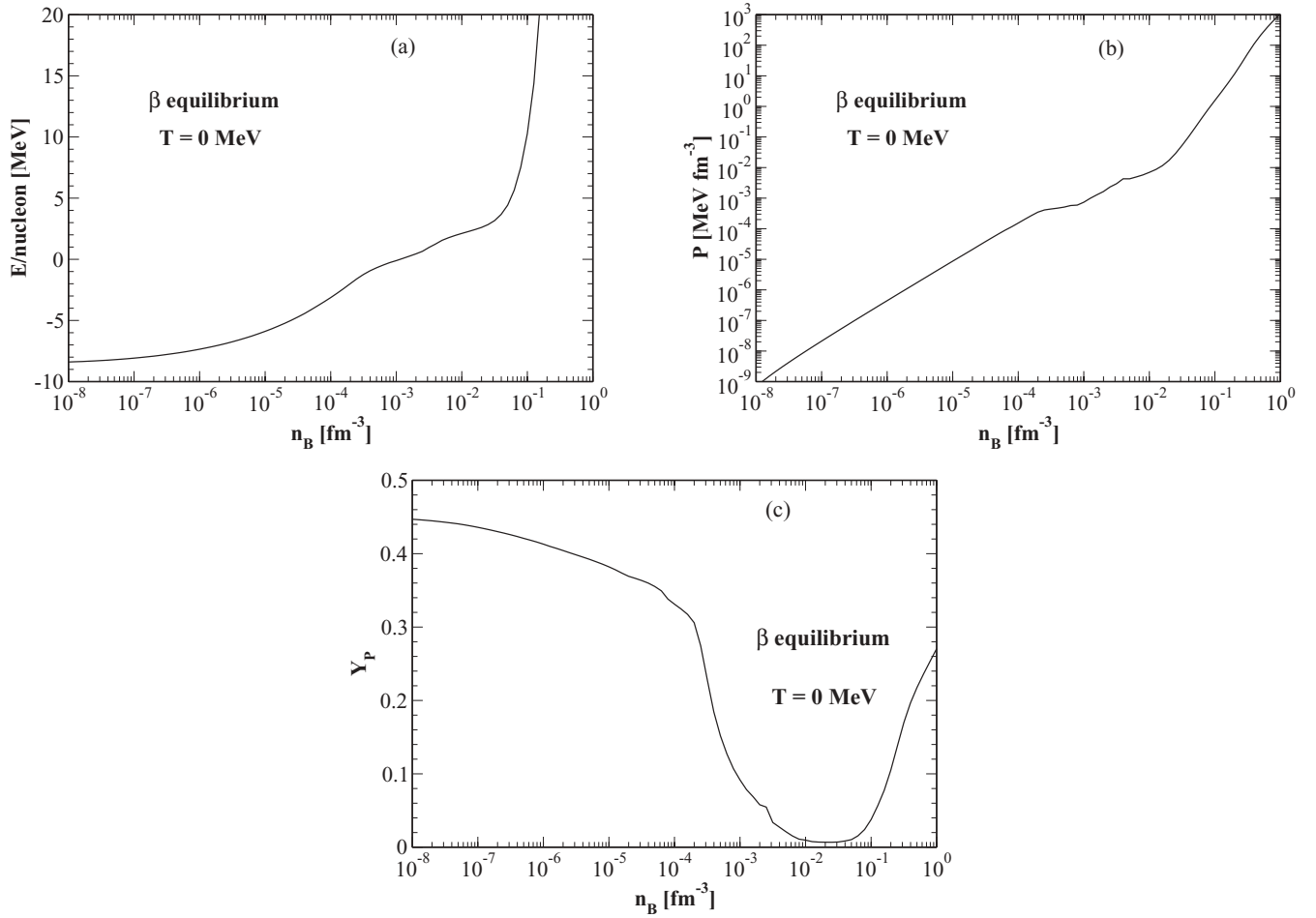
FIG. 14. (a) Energy, (b) pressure, and (c) proton fraction vs density for $T = 0$ nuclear matter in chemical equilibrium.

test result for the S-S EOS is also shown (as a dot-dashed curve) for the similar initial condition. Note that it is important to use an accurate interpolation scheme with the EOS table to ensure

that the first law is satisfied so that entropy is conserved. The adiabatic compression test result for the S-S EOS was obtained using the routine developed in Ref. [22].

IV. SUMMARY AND OUTLOOK

In this paper we generate a new complete EOS for use in supernova and neutron star merger simulations. We use a density-dependent RMF model for nuclear matter at intermediate and high density with a spherical Wigner-Seitz approximation for nonuniform matter, which incorporates nuclear shell effects [4]. For nuclear matter at low density [5], we use a virial expansion for a nonideal gas consisting of neutrons, protons, α particles, and thousands of heavy nuclei from the finite range droplet model (FRDM) mass table [18]. We include second-order virial corrections for light elements $A \leqslant 4$, nuclear partition functions for heavy nuclei, and Coulomb corrections between electrons and heavy nuclei. As the density decreases, the mean field results match smoothly to the virial gas. As the density goes down, the virial expansion reduces to nuclear statistical equilibrium and the virial expansion is exact in the low-density limit. The computed EOS covers 180 000 grid points in the temperature range $T = 0$–80 MeV, the density range $n_B = 10^{-8}$–1.6 fm^{-3}, and the proton fraction range $Y_P = 0$–0.56.
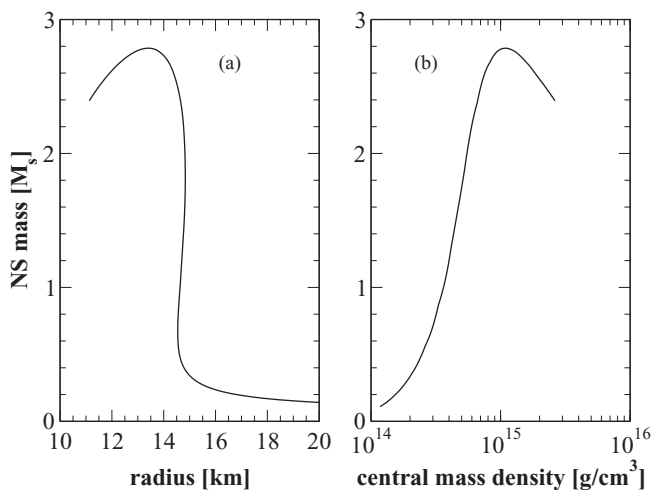

FIG. 15. (a) Mass vs radius and (b) mass vs central density for neutron star from $T = 0$ β equilibrium nuclear matter as shown in Fig. 14.

We use a hybrid interpolation scheme to generate a full EOS table on a fine grid that is thermodynamically consistent. This ensures that the first law of thermodynamics is satisfied and that entropy is conserved during adiabatic compression. Our EOS is an improvement over the existing L-S [11] and S-S [12,13] EOSs because our EOS includes thousands of heavy nuclei and is exact in the low-density limit.

We discuss the thermodynamic properties of our EOS in detail. The free energy per baryon, pressure, entropy per baryon, and chemical potentials for neutrons, protons, and electron neutrinos are shown for matter at high and low temperatures and for large and small proton fractions. We also perform adiabatic compression tests for our EOS table and show that it preserves entropy to better than 1%.

Finally, we show some comparisons between our EOS and two existing EOS tables. At high density, our RMF model reduces to the normal NL3 set. It produces a stiffer EOS at high density than the S-S EOS, which is already stiffer than the L-S EOS. One can find this difference, for example, in Fig. 16 for the pressure at high density. As a result, neutron stars obtained from our EOS have a large maximum mass of around 2.77 solar mass and radius of 13.3 km. At low density, our model is essentially the virial expansion of a nonideal gas, which includes many nuclei. Our model usually has a broad distribution of nuclei as shown in our previous paper [5]. This spread in the distribution of nuclei makes the composition of nuclear matter in our EOS different from that in the L-S and S-S EOS tables. This composition difference also introduces some differences in the entropy for nuclear matter at a low temperature and large proton fraction; see, for example, Fig. 19(b) for matter with $T = 1$ MeV and $Y_P = 0.4$. More importantly, the composition of nuclear matter, especially the wide spreads in distribution of nuclei, could influence the position of the neutrinosphere and the spectra of radiated neutrinos and antineutrinos.

The complete EOS table is useful not only for core-collapse supernova simulations but also for other astrophysical applications, including the long-term evolution of protoneutron stars and neutron star mergers. Our procedure, for matching mean-field and virial calculations to produce a thermodynamically consistent EOS, can be used for a variety of effective interactions. In this paper we have presented an EOS based on the NL3 interaction that is relatively stiff at high densities. In future work we will present additional EOS tables based on softer interactions that have lower pressures at high densities.

Finally, our full EOS tables, both with and without lepton and photon contributions, are available for download as described in the Appendix.

APPENDIX: FORMAT OF EOS TABLES

Here we describe the physical quantities provided in the tables for the EOS, NL3eos1.03.dat and NL3eosb1.03.dat, and where they can be downloaded. One should download the gzip compressed files NL3eos1.03.dat.gz and NL3eosb1.03.dat.gz (which are about 100 MB each) and use gunzip to decompress them. The grid structures of these tables are indicated in Table II and contain approximately 517 MB of data each. The tables, a sample FORTRAN computer program, and a readme file are available for download both at our Web site http://cecelia.physics.indiana.edu/gang_shen_eos/ and we expect, from the Electronic Physics Auxiliary Publication Service—EPAPS Web site [23]. Please check our Web site for any updated information regarding these EOS tables.

The tables contain a number of quantities. For a single triplet of T, n_B, and Y_P, there are 16 items that make up a row of the table. These items are described below. In the table NL3eosb1.03.dat, only the contribution from baryons is taken into account for items 4, 5, and 6. In the table NL3eos1.03.dat, the contributions from electrons, positrons, and photons are also included. The electron mass is 0.511 MeV.

A. Items in EOS tables

(i) Temperature T (MeV). The range of temperature is first $T = 0$ then from $10^{-0.8} - 10^{1.875}$ MeV; see Table II.

(ii) Proton fraction Y_P. The range of proton fraction is first 0, and then from, 0.05–0.56. The step in proton fraction is 0.01; see Table II.

(iii) Baryon number density n_B (fm^{-3}). The range of density is from 10^{-8} to $10^{0.175}$ fm^{-3}; see Table II.

(iv) Free energy per baryon, F/A (MeV), in which the free nucleon mass of 939 MeV has been subtracted.

(v) Pressure P (MeV/fm^3).

(vi) Entropy per baryon, S/A (k_B).

(vii) Chemical potential for neutrons, μ_n (MeV). The tabulated value is relative to the nucleon mass of 939 MeV.
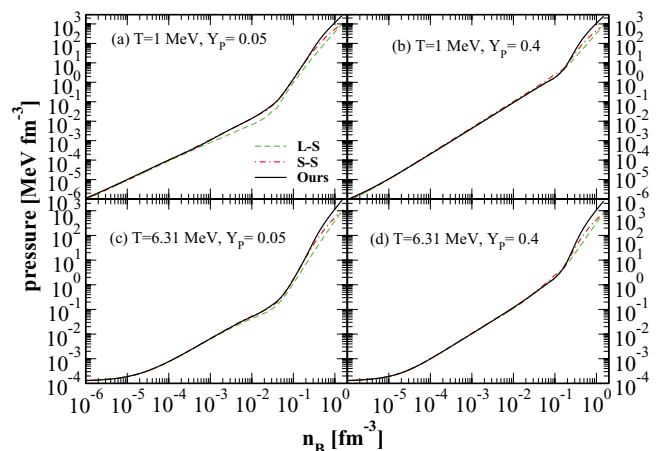

FIG. 16. (Color online) Pressure ves baryon density from our, L-S's, and S-S's EOSs with (a) $T = 1$ MeV and $Y_p = 0.05$, (b) $T = 1$ MeV and $Y_p = 0.4$, (c) $T = 6.31$ MeV and $Y_p = 0.05$, and (d) $T = 6.31$ MeV and $Y_p = 0.4$.
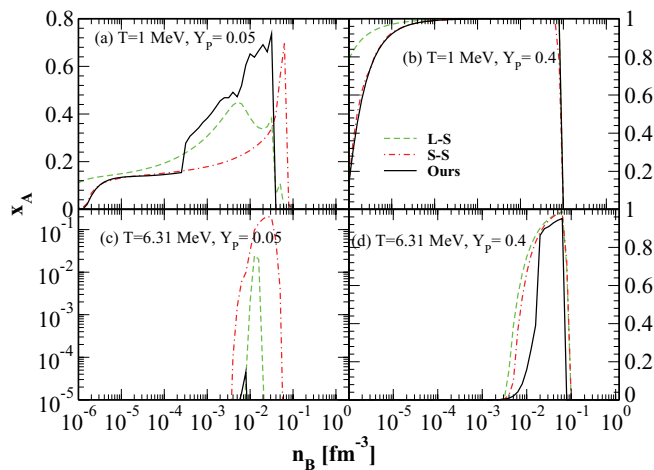
FIG. 17. (Color online) Mass fraction of heavy nuclei versus baryon density from our, L-S's, and S-S's EOSs with (a) $T = 1$ MeV and $Y_p = 0.05$, (b) $T = 1$ MeV and $Y_p = 0.4$, (c) $T = 6.31$ MeV and $Y_p = 0.05$, and (d) $T = 6.31$ MeV and $Y_p = 0.4$.

FIG. 19. (Color online) Average mass number A (black upper curves) and atomic number Z (red lower curves) of heavy nuclei for our (solid), L-S's (dot-dashed), and S-S's (dashed) EOSs for $T = 1$ MeV and $Y_P = 0.4$.

(viii) Chemical potential for protons, μ_p (MeV). The tabulated value is relative to the nucleon mass.

(ix) Chemical potential for electrons, μ_e (MeV). The tabulated value includes the electron mass.

(x) Average mass number $\bar{A}$ of heavy nuclei with $A > 4$, which exclude α particles.

(xi) Average proton number $\bar{Z}$ of heavy nuclei with $A > 4$, which exclude α particles.

(xii) Mass fraction of free neutrons.

(xiii) Mass fraction of free protons.

(xiv) Mass fraction of α particles.

(xv) Mass fraction of heavy nuclei with $A > 4$, which exclude α particles.

(xvi) Effective nucleon mass M^* (MeV). In uniform matter it is obtained from RMF theory. For virial gas and

nonuniform matter, it is chosen to be the free nucleon mass $M^* = 939$ MeV.

B. Sample FORTRAN computer program readeos.f

The FORTRAN program readeos.f includes a very short main program that calls the subroutine load_table to read NL3eos1.03.dat or NL3eosb1.03.dat, and then calls the subroutine readeos with inputs T (MeV), proton fraction Y_p, and density n (fm^{-3}). The subroutine readeos uses trilinear interpolation (in T, Y_p, and n) to return the above 16 values plus the internal energy per baryon (MeV) and the chemical potential for electron neutrinos in chemical equilibrium (MeV). Note that one needs to call load_table only once, and then one can call readeos many times. For further details, see the comments in readeos.f.
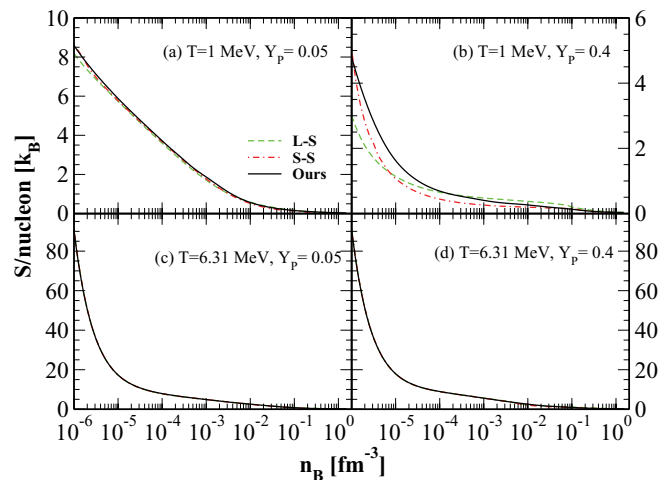

FIG. 18. (Color online) Entropy per baryon vs baryon density from our, L-S's, and S-S's EOSs with (a) $T = 1$ MeV and $Y_P = 0.05$, (b) $T = 1$ MeV and $Y_P = 0.4$, (c) $T = 6.31$ MeV and $Y_P = 0.05$, and (d) $T = 6.31$ MeV and $Y_P = 0.4$.
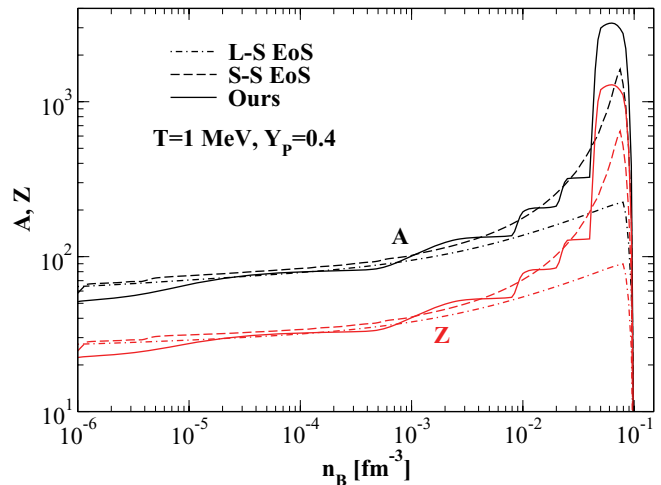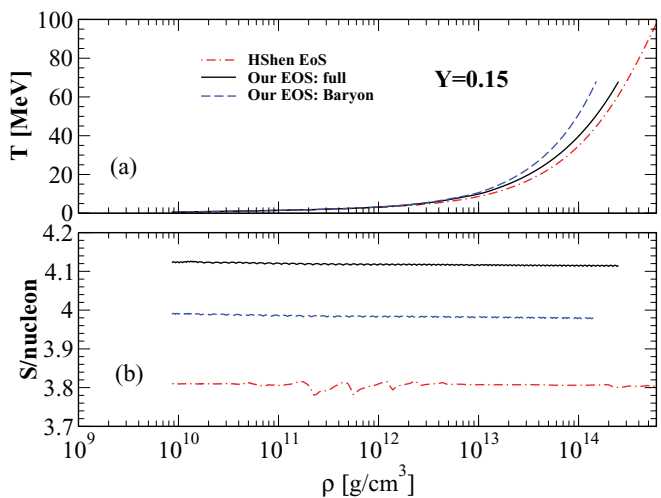

FIG. 20. (Color online) (a) Temperature and (b) entropy vs density in the adiabatic compression for nuclear matter with fixed proton fraction 0.15.

[1] H.-Th. Janka, K. Langanke, A. Marek, G. Martínez-Pinedo, and B. Müller, Phys. Rep. **442**, 38 (2007).

[2] A. Arcones, G. Martínez-Pinedo, E. O'Connor, A. Schwenk, H.-T. Janka, C. J. Horowitz, and K. Langanke, Phys. Rev. C **78**, 015806 (2008).

[3] See, for a recent review, H. Duan, G. M. Fuller, and Y.-Z. Qian, Ann. Rev. Nucl. Part. Sci. **60**, 569 (2010).

[4] G. Shen, C. J. Horowitz, and S. Teige, Phys. Rev. C **82**, 015806 (2010).

[5] G. Shen, C. J. Horowitz, and S. Teige, Phys. Rev. C **82**, 045802 (2010).

[6] C. J. Horowitz and A. Schwenk, Nucl. Phys. A **776**, 55 (2006).

[7] C. J. Horowitz and A. Schwenk, Phys. Lett. B **638**, 153 (2006).

[8] C. J. Horowitz and A. Schwenk, Phys. Lett. B **642**, 326 (2006).

[9] C. J. Horowitz, Phys. Rev. D **55**, 4577 (1997).

[10] S. Typel, G. Röpke, T. Klähn, D. Blaschke, and H. H. Wolter, Phys. Rev. C **81**, 015803 (2010).

[11] J. M. Lattimer and F. D. Swesty, Nucl. Phys. A **535**, 331 (1991).

[12] H. Shen, H. Toki, K. Oyamatsu, and K. Sumiyoshi, Nucl. Phys. A **637**, 435 (1998).

[13] H. Shen, H. Toki, K. Oyamatsu, and K. Sumiyoshi, Prog. Theor. Phys. **100**, 1013 (1998).

[14] G. A. Lalazissis, J. König, and P. Ring, Phys. Rev. C **55**, 540 (1997).

[15] Jim Lattimer (private communication, 2009).

[16] We thank C. Ott for providing us with the subroutine for 1D cubic Hermite interpolation with slope limiter.

[17] W. H. Press, B. P. Flannery, S. A. Teukolsky, and W. T. Vetterling, *Numerical Recipes* (Cambridge University Press, Cambridge, 1989), pp. 95–101.

[18] P. Möller, J. R. Nix, and W. J. Swiatecki, At. Data Nucl. Data Tables **59**, 185 (1995).

[19] J. R. Oppenheimer and G. M. Volkoff, Phys. Rev. **55**, 374 (1939).

[20] R. C. Tolman, Phys. Rev. **55**, 364 (1939).

[21] G. Baym, C. Pethick, and P. Sutherland, Astrophys. J. **170**, 299 (1971).

[22] E. O'Connor and C. D. Ott, Class. Quantum Grav. **27**, 114103 (2010).

[23] See supplemental material at [http://link.aps.org/supplemental/10.1103/PhysRevC.83.035802].